Vapor–liquid phase coexistence curves for Morse fluids

Jayant K. Singh [a],*, Jhumpa Adhikari [b], Sang Kyu Kwak [c]

[a] *Department of Chemical Engineering, Indian Institute of Technology Kanpur, Kanpur 208016, India*
[b] *Department of Chemical Engineering, Indian Institute of Technology Bombay, Powai, Mumbai 400076, India*
[c] *Division of Chemical and Biomolecular Engineering, School of Chemical and Biomedical Engineering,*
Nanyang Technological University, Singapore 637722, Singapore

Abstract

Phase coexistence of Morse fluids is predicted for parameters in the range describing the behavior of metals using the grand-canonical transition matrix Monte Carlo method. The critical properties of the vapor–liquid equilibrium curves for three fcc metals, Al, Cu, and Au, and two bcc alkali metals, Na and K, are estimated and the critical temperature values are found to be in good agreement with the experimental data for the fcc metals considered but overestimated for the bcc metals. For Na, it was found that the critical density and vapor pressure as a function of temperature (below the critical temperature) estimates to be approximately concurrent with experimental results.
© 2006 Elsevier B.V. All rights reserved.

1. Introduction

The Morse potential energy function (PEF) is well suited to describe the effective pair interaction forces in diatomic molecules [1,2] and metals [3–6]. The vapor–liquid equilibrium (VLE) curves for this PEF have not been studied extensively. Okumura and Yonezawa [7] predicted the VLE for this potential model by scaling with respect to the separation $r_{min} = 2^{1/6}\sigma$ where Lennard-Jones (LJ) energy is at its minimum and obtained reduced critical temperature $T_C^* = kT_C/D = 0.928$, pressure $P_C^* = P_C\sigma^3/D = 0.331$, and density $\rho_C^* = \rho_C\sigma^3 = 0.084$, where σ is the LJ diameter and D is the energy parameter for the Morse potential. The aim of the study is to add to the understanding of the coexistence properties of the Morse potential model for the range of parameters describing metals without using the LJ scaling parameter, r_{min}. Morse originally developed this pair PEF to correctly describe the allowed vibrational energy levels in diatomic molecules [1]. Girifalco and Weizer extended the application of the Morse potential to model cubic metals [4]. Lincoln, et al. further refined the Morse potential for

the five metals, which are studied here, by fitting the parameters to experimentally determined values of the lattice constant, bulk modulus, and cohesive energy [3]. The authors then theoretically predicted the elastic constants and found the values to be in good agreement with experimental data. The Morse potential has also been used to model the formation and diffusion of the vacancies in carbon, silicon, and germanium [8]. Ruffa has used this potential model to hypothesize the association of melting in cubic metals with the maximum allowable thermal expansion in the solid metal [5] and also determined the dependence of elastic shear moduli on the aforementioned thermal expansion properties [6].

Metals at room temperature and pressure are generally solids with the exception of mercury. However, at extreme conditions of temperature and pressure, metals exist in the liquid and vapor phases. In the liquid phase, the metal melt consists of ions and delocalized electrons. The vapor phase consists of isolated atoms at low densities. At high densities, near the critical point, the metal vapor contains ions and unbound electrons [9]. We have simplified all the possible interparticle interactions in the liquid and vapor phases of the metals such that the interactions are effectively modeled by using the Morse potential. The VLE curves of alkali metals, sodium (Na), and potassium (K) forming body-centered-cubic (bcc) lattice in the solid state, have been determined to compare with available experimental data. For the

* Corresponding author.
E-mail addresses: jayantks@iitk.ac.in (J.K. Singh), adhikari@che.iitb.ac.in (J. Adhikari), skkwak@ntu.edu.sg (S.K. Kwak).

metals, aluminum (Al), gold (Au), and copper (Cu), which form stable face-centered-cubic (fcc) lattice in the solid state, the VLE data has been predicted. The equilibrium curves for the metal melt and vapor have been predicted in this study using the grand-canonical transition-matrix Monte Carlo (GC-TMMC) method [10].

2. Potential model

Mathematically, the Morse function is expressed as:

$$U(r_{ij}) = D[e^{-2\alpha(r_{ij}-r_0)} - 2 e^{-\alpha(r_{ij}-r_0)}], \qquad (1)$$

where the constant D is the dissociation energy, α a constant with dimensions of reciprocal length, and r_0 is the equilibrium distance of the two particles. The distance between the ith and jth particles is given by r_{ij}. At $r_{ij} = r_0$, the minimum energy is given by $U(r_0) = -D$. The parameters D, α, and r_0 have been determined by a fitting procedure to experimental data for the lattice constant, bulk modulus, and cohesive energies of the respective metals in their solid states at room temperature [3]. The same values for these parameters are used to model the VLE curves for these metals. Table 1 exhibits the parameters for the five metals used in the study. The range of interactions for the bcc metals studied is much higher than that for the fcc metals as is reflected in the values of the α parameters. The quantity αr_0 for the five metals under our consideration lies in a narrow range from 2.95 to 4.79. However, the steepness of the potential is higher for the fcc metals as compared to the bcc metals as is expected from the values for D. The use of a pair potential model simplifies the computations and the results of simulations, has been shown to successfully predict the elastic constants for metals [3].

3. Simulation method and details

Simulations are conducted in the grand canonical ensemble where the chemical potential μ, volume V, and temperature T are kept fixed and particle number N and energy U fluctuate. The probability π of observing a microstate s with energy U_s and particle number N_s is:

$$\pi_s = \frac{1}{\Xi} \frac{V^{N_s}}{\Lambda^{3N_s} N_s!} \exp[-\beta(U_s - \mu N_s)], \qquad (2)$$

where $\beta = 1/k_B T$ is the inverse temperature, Ξ the grand canonical partition function, and Λ is the de Broglie wavelength. The probability $\Pi(N)$ of observing a macrostate with a given number of molecules (density) is given by:

$$\Pi(N) = \sum_{N_s=N} \pi_s. \qquad (3)$$

To obtain the probability distribution $\Pi(N)$ we employ the transition matrix Monte Carlo scheme [10], with a N-dependent sampling bias. The method monitors the acceptance probability of attempted MC moves and subsequently uses this information to calculate the macrostate transition probability matrix. For every attempted move from a microstate s to a microstate t, regardless of whether the move is accepted, we update a collection matrix C with the acceptance probability $a(s \to t) = \min[1, \pi_t/\pi_s]$ as follows:

$$\begin{aligned} C(N \to M) &= C(N \to M) + a(s \to t), \\ C(N \to N) &= C(N \to N) + 1 - a(s \to t), \end{aligned} \qquad (4)$$

where N and M represent the macrostate labels for microstates s and t, respectively. At any time during the simulation the macrostate transition probability matrix can be obtained by appropriately normalizing the collection matrix:

$$P(N \to M) = \frac{C(N \to M)}{\sum_O C(N \to O)}. \qquad (5)$$

To obtain the macrostate probabilities, we utilize the detailed balance expression:

$$\Pi(N)P(N \to M) = \Pi(M)P(M \to N). \qquad (6)$$

For a grand-canonical simulation where transitions in N are such that $N \to N$, $N \to N+1$, and $N \to N-1$, the transition-probability matrix P is tri-diagonal. In such conditions, a sequential approach provides a suitable means for obtaining the macrostate probabilities:

$$\ln \Pi(N+1) = \ln \Pi(N) - \ln \left[\frac{P(N+1 \to N)}{P(N \to N+1)} \right]. \qquad (7)$$

To ensure adequate sampling of all states we employ a multi-canonical sampling [11] scheme that encourages the system to sample all densities with uniform frequency. This procedure is implemented by assigning each macrostate a weight $\eta(N)$ that is inversely proportional to the current estimate of its probability, $\eta(N) = -\ln \Pi(N)$. Acceptance criteria are modified to account for the bias as follows:

$$a_\eta(s \to t) = \min \left[1, \frac{\eta(M)\pi_t}{\eta(N)\pi_s} \right], \qquad (8)$$

where $\eta(N)$ and $\eta(M)$ are weights corresponding to microstates s and t, respectively. Introduction of a weighting function does not alter the mechanism through which the collection matrix is updated. The unbiased acceptance probability is still used to update the collection matrix.

Simulations are completed at a specified value of the chemical potential, which is not necessarily close to the saturation value. To determine the phase-coexistence value of the chemical potential, the histogram reweighting method of Ferrenberg and Swendson [12] is used. This method enables one to shift

Table 1
Parameters for Morse potential energy function [3]

Metal	D ($\times 10^{-13}$ ergs)	α (Å^{-1})	r_0 (Å)	αr_0
Al	4.3264	1.0341	3.4068	3.5230
Cu	5.2587	1.3123	2.8985	3.8037
Au	7.6148	1.5830	3.0242	4.7873
Na	0.9241	0.5504	5.3678	2.9544
K	0.8530	0.4766	6.4130	3.0564

the probability distribution obtained from a simulation at chemical potential μ_0 to a probability distribution corresponding to a chemical potential μ using the relation:

$$\ln \Pi(N; \mu) = \ln \Pi(N; \mu_0) + \beta(\mu - \mu_0)N. \tag{9}$$

To determine the coexistence chemical potential, we apply the above relation to find the chemical potential that produces a probability distribution $\Pi_c(N)$ where the areas under the vapor and liquid regions are equal. Saturated densities are related to the first moment of the vapor and liquid peaks of the coexistence probability distribution. To calculate the saturation pressure we use the expression:

$$\beta pV = \ln \left(\sum_N \frac{\Pi_c(N)}{\Pi_c(0)} \right) - \ln(2). \tag{10}$$

The critical properties are estimated from a least square fit of the scaling law:

$$\rho^l - \rho^v = C_1 \left(1 - \frac{T}{T_c}\right)^{\beta_c} + C_2 \left(1 - \frac{T}{T_c}\right)^{\beta_c + \Delta}, \tag{11}$$

where ρ^l and ρ^v are the liquid and vapor densities, respectively, and C_1 and C_2 are fitting parameters. The critical exponent β_c is taken as 0.325 and $\Delta = 0.51$. The critical temperature estimate from the above is utilized to get the critical density from the least square fit to the law of rectilinear diameter [13]:

$$\frac{\rho^l + \rho^v}{2} = \rho_c + C_3(T - T_c). \tag{12}$$

Critical pressure is calculated using the least square fitting to the following expression:

$$\ln P = A - \frac{B}{T + C} \tag{13}$$

where A and B are constants.

Simulations for calculating saturated densities and vapor pressures are conducted using single AMD Opteron. The MC move distribution is: 30% particle displacement, 35% particle insertion and 35% particle deletion. Typical maximum molecule numbers for these simulations varied from 350 to 550. Finite size effects on the phase coexistence densities and vapor pressures are observed to become negligible for system size (maximum number of molecules) above 350 for all the metals. For each data point, four runs were performed to calculate the statistical error.

4. Results and discussion

Fig. 1 shows typical probability density curves for Na. As the temperature increases, the free energy barrier between the coexisting vapor and liquid phases (shown as two peaks in Fig. 1) decreases. This barrier disappears at the critical point. The simulation results for the Morse fluids using parameters listed in Table 1 are summarized in Table 2 in terms of chemical potential, pressure, and densities of the vapor and liquid phases at coexistence for the temperatures of interest. The VLE curves of the Morse potential model for the fcc metals, Al, Cu, and Au, and for the bcc metals, Na and K, are illustrated in Figs. 2 and 3.
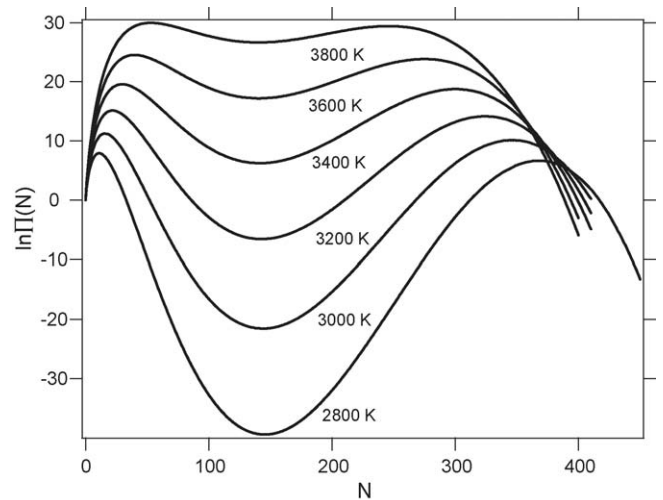

Fig. 1. Plot of probability densities of Na vs. molecule number, N, over the temperature range from 2800 to 3800 K with interval of 200 K. Statistical error is smaller than the symbol size.

Fig. 2 presents the plot of reduced temperature ($T_r = T/T_C$) versus reduced density ($\rho_r = \rho/\rho_C$). It shows that the saturated liquid lines for the fcc metals are displaced from those representing the bcc metals whereas the saturated vapor lines are almost concurrent for all the metals. The ratio of reduced density ρ_{r1} of any metal taken with respect to the minimum value for reduced density, ρ_{r2}, leads to the observation that at $T_r = 0.7 \rho_{r1}/\rho_{r2}$ of vapor phase is approximately twice than that of liquid phase. However, absolute difference $|\rho_{r1} - \rho_{r2}|$ is greater in the liquid-phase and is likely to reflect the differences in structure of the fcc and bcc metals whereas in the vapor phase no such differences would exist. The critical compressibility factor Z_C is given by $Z_C = P_C V_C / RT_C$ and values of Z_C for the five metals studied here are given in Table 3. The behavior of the Morse vapor indicates significant deviation from ideal gas behavior at the critical point. The corresponding states theorem states that the reduced densities at the same T_r, P_r for vapors, with same acentric factor,
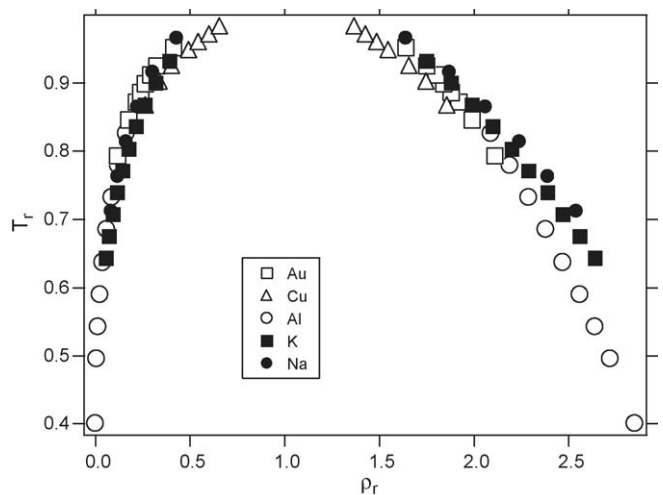

Fig. 2. VLE curves for Al, Cu, Au, Na, and K. Temperature and density values are reduced by critical properties; the reduced temperature, $T_r = T/T_C$ and the reduced density, $\rho_r = \rho/\rho_C$. Statistical error is smaller than the symbol size.

Table 2
Summary of simulation results indicating the chemical potential, pressure, and densities in the vapor and liquid phases at coexistence for each metal

Metal	T (K)	$\beta\mu$	P (bar)	ρ_v (kg/m³)	ρ_l (kg/m³)
	3400	−10.661 (5)	11.06 (8)	1.066 (8)	2254 (14)
	4200	−8.9520 (9)	76.85 (7)	6.106 (5)	2130 (7)
	4600	−8.3423 (1)	157.3 (1)	11.60 (2)	2070 (2)
	5000	−7.8428 (5)	287.4 (1)	19.91 (15)	2010 (3)
	5400	−7.4315 (5)	479.0 (4)	31.69 (3)	1940 (5)
Al	5800	−7.0832 (6)	748.8 (6)	47.52 (6)	1870 (1)
	6200	−6.7868 (3)	1109 (1)	68.54 (5)	1800 (2)
	6600	−6.5424 (5)	1569 (1)	95.42 (2)	1720 (1)
	7000	−6.3220 (4)	2127 (1)	128.6 (1)	1639 (1)
	7200	−6.2226 (2)	2460 (1)	149.4 (1)	1600 (1)
	7400	−6.1298 (1)	2825 (1)	172.8 (1)	1550 (1)
	7500	−5.6688 (3)	4668 (2)	706 (1)	4910 (3)
	7800	−5.5436 (2)	5678 (1)	898 (1)	4610 (2)
	8000	−5.4671 (2)	6423 (5)	1070 (1)	4380 (1)
Cu	8200	−5.3938 (3)	7254 (3)	1310 (4)	4080 (5)
	8300	−5.3597 (2)	7684 (4)	1440 (6)	3920 (4)
	8400	−5.3261 (2)	8140 (4)	1590 (5)	3760 (3)
	6000	−6.5460 (1)	1419 (1)	702 (1)	12500 (7)
	6400	−6.2715 (2)	2086 (1)	1050 (1)	11800 (4)
	6600	−6.1463 (1)	2504 (1)	1280 (1)	11400 (4)
	6700	−6.0891 (1)	2726 (1)	1420 (1)	11200 (8)
Au	6800	−6.0334 (2)	2963 (2)	1570 (2)	10900 (9)
	6900	−5.9807 (1)	3213 (1)	1740 (1)	10700 (4)
	7000	−5.9297 (1)	3478 (1)	1930 (1)	10400 (6)
	7200	−5.8322 (2)	4058 (1)	2415 (2)	9744 (8)
	2800	−7.4748 (1)	252.6 (1)	29.57 (1)	900.5 (2)
	3000	−7.2115 (2)	364.7 (2)	41.93 (3)	846.8 (2)
Na	3200	−6.9869 (2)	505.2 (1)	57.90 (3)	792.1 (7)
	3400	−6.7933 (2)	677.3 (3)	78.78 (7)	731.4 (7)
	3600	−6.6253 (1)	883.2 (2)	107.4 (1)	664.6 (4)
	3800	−6.4789 (5)	1126 (1)	152.3 (1)	581.3 (3)
	2000	−8.5429 (3)	59.79 (1)	15.88 (1)	735.5 (2)
	2100	−8.3319 (4)	79.10 (4)	20.53 (1)	712.7 (1)
	2200	−8.1426 (1)	102.3 (1)	26.08 (1)	688.7 (1)
	2300	−7.9728 (4)	129.6 (1)	32.64 (2)	663.9 (11)
K	2400	−7.8192 (2)	161.3 (1)	40.39 (1)	638.4 (5)
	2500	−7.6811 (2)	197.5 (1)	49.44 (1)	612.6 (3)
	2600	−7.5547 (1)	238.9 (1)	60.21 (1)	585.4 (4)
	2700	−7.4395 (3)	285.4 (2)	73.09 (5)	555.5 (6)
	2800	−7.3339 (2)	337.4 (2)	88.89 (4)	523.6 (3)

Subscripts 'v' and 'l' represent vapor and liquid, respectively. Numbers in the parenthesis indicate 67% confidence limits of the last digit(s) of the reported value.

Table 3
Critical compressibility factors from simulation

Metal	Z_C
Al	0.2485 (20)
Cu	0.3203 (60)
Au	0.2808 (16)
Na	0.2583 (40)
K	0.2893 (54)

Numbers in the parenthesis indicate 67% confidence limits of the last digits of the reported value.
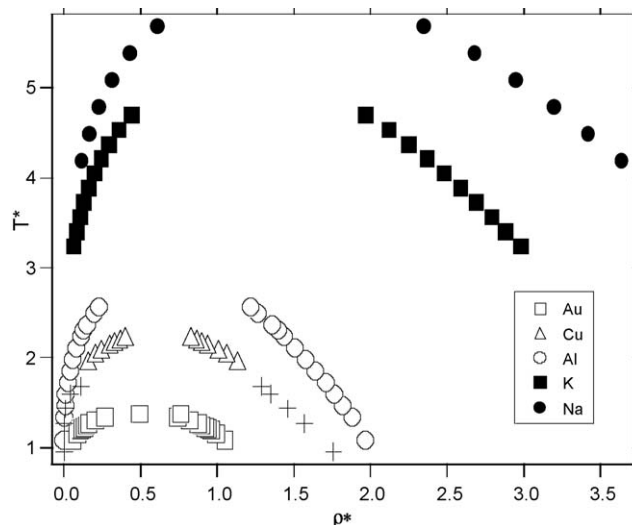

Fig. 3. VLE curves for Al, Cu, Au, Na, and K. The reduced temperature and density are $T^* = kT/D$ and $\rho^* = \rho r_0^3$, respectively. Statistical error is smaller than the symbol size. Symbol "+" represents the results of Bhatt et al. [19].

deviate from ideal gas behavior by the same amount. The acentric factor is determined by using an expression given below:

$$\omega = -1.0 - \log(P_r^{sat})_{T_r=0.7}. \tag{14}$$

The experimental value for acentric factor of Na is −0.13 and our simulation results predict an acentric factor of −0.25. The Morse potential is able to predict qualitatively that the acentric factor for Na vapor is negative. Limited experimental data does not allow comparison for the other metals. The metal vapors are anticipated to behave drastically differently from simple fluids, for which $\omega = 0$, and the Morse potential is able to predict this difference. The increase in the value of αr_0 for the metals from Na to Au becomes evident in Fig. 3 as a corresponding decrease in critical temperature and critical density. The estimated temperature, density, and pressure at critical point from simulations and the known values from experiments for all five metals are shown in Table 4. Comparison with available reference data shows the calculated critical temperature for the fcc metals to be within 13% deviation from the literature value, though the critical temperature is overestimated for both the bcc metals. The critical pressure and critical density values as determined by our simulations for all the five metals are of the same order as the values found in literature though considerably overestimated. The critical pressure values for Au and Al, and critical density value for Na are exceptions. Note that the critical point data for the metals show considerable scatter in literatures [14–16].

The vapor pressures for all the metals in the given temperature range have also been estimated from the simulation. Fig. 4 shows the plot of logarithmic saturation pressures with the inverse temperature and exhibits linear relations below the critical pressure. Hence, the Antoine formalism given by Eq. (13) is used to determine the critical pressure instead of the more complex Wagner equation. The differences in the nature of the bcc and the fcc metals are reflected in the behavior of the respective vapor pressures as related to temperature. The critical temperature range

Table 4
Summary of critical properties from simulation and literature

Metal	Simulation			Literature		
	T_C (K)	P_C (bar)	ρ_C (kg/m^3)	T_C (K)	P_C (bar)	ρ_C (kg/m^3)
Al[a]	8472 (50)	5094 (40)	785 (8)	8944	4726	430
Cu[a]	8650 (50)	9543 (180)	2631 (3)	7696	5829	1930
Au[b]	7566 (30)	5250 (30)	5925 (5)	7400 (1100)	5300 (200)	7692 (1775)
Na[c]	3932 (10)	1290 (20)	353 (2)	2485	248	300
K[c]	3120 (10)	534 (10)	277 (1)	2280	161	190

Numbers in the parenthesis under the title 'simulation' indicate 67% confidence limits of the last digit(s) of the reported value. Error values for literature data are shown wherever it was available.

  [a] Reference [14].
  [b] Reference [22].
  [c] Reference [23].

of Al extrapolated from experimental data is observed from 5700 to 12,100 K [17,18]. The recent study by Bhatt et al. using the Gibbs ensemble Monte Carlo technique with the complex embedded-atom potential (called NP-B potential) reveals a critical temperature of 6299 K [19]. The critical temperature of Al from our simulation (see Table 4) shows a higher value than Bhatt et al.'s, yet both values lies within the reported experimental range. Our simulation result shows good agreement with some of the literature values [20,21]. Note that literature values of the critical point for fcc metals except Au are obtained from fitting procedures to experimental data. Experimental data available for Na (see Fig. 5) shows that the values of the saturation pressures from experiment and simulation follow a same trend. However, the vapor pressure is underestimated consistently by our simulation. From Table 4, the estimated Na critical density of 353 kg/m^3 is close to the experimental value of 300 kg/m^3. This is however not true for K, where the predicted critical density is higher than the experimental value. The critical pressures for the alkali metals show large deviations from the experimental values. For Na, the pressure is vastly overestimated because the critical temperature is overvalued. It is observed that at the experimental critical point of Na metal, 2485 K, the correspond-
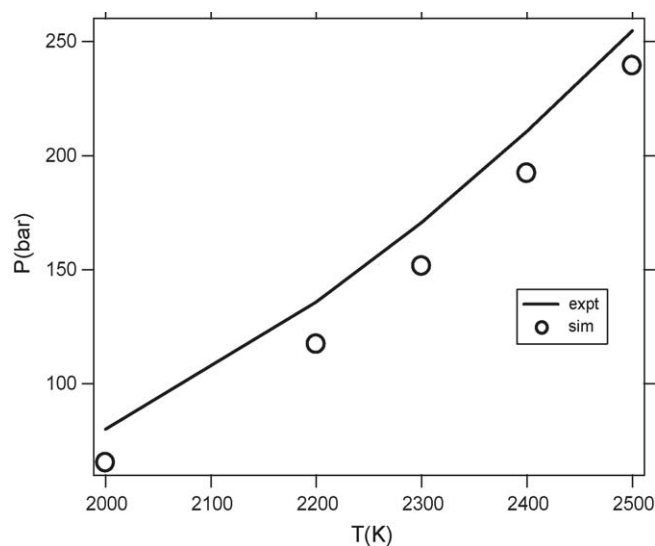

Fig. 5. Comparison plot of vapor pressures for Na as a function of temperature between simulation and experimental values.

ing pressure predicted by simulation is a good approximation to the experimental critical pressure.

5. Conclusions

Availability of experimental data for Na has allowed for comparisons with our simulation results and except for the critical point (T_C, P_C), simulated values of vapor pressure as a function of temperature closely follow the experimental data. The experimental critical properties of K are much lower than those estimated from the Morse potential. The VLE data for the fcc metals has also been predicted. The limited literature data available does not allow for a comprehensive comparison. The critical temperatures estimated for Al, Cu, and Au, lie within 13% of the literature values. The critical pressure and critical density simulation values for the three fcc metals are overestimated, with the exception of critical pressure values for Au and Al as noted in the previous section. The differences in the structures of the metal melt for the fcc and bcc metals are also reflected in the VLE curves.
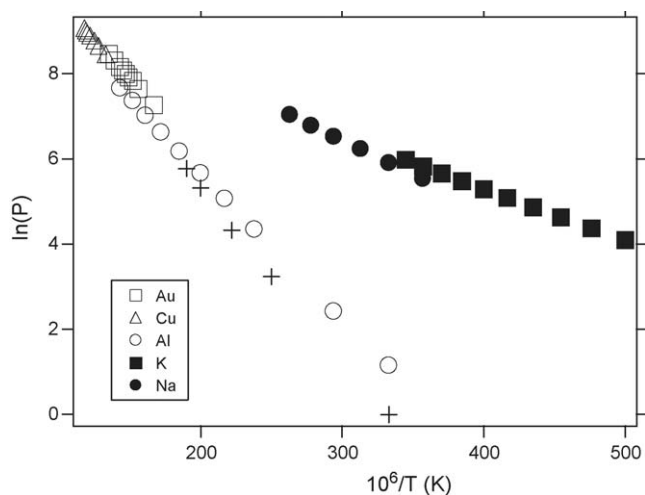

Fig. 4. Plot of saturation pressure as a function of inverse temperature. Statistical error is smaller than the symbol size. Symbol "+" represents the results of Bhatt et al. [19].

In this study, a simple pair PEF, the Morse potential model, with the fitting parameters reflecting solid phase properties has been used to interpret the complex interactions in the liquid and vapor phases. The Morse PEF has been combined with a classical Monte Carlo technique, GC-TMMC, to predict the VLE for metals in forms of fluids. The objectives of the study were to investigate the behavior of Morse fluids and how correctly the solid phase parameters available in literature describe the vapor and liquid phases, which are distinctly different in behavior from the solid phase. Since the Morse PEF is not completely reducible, the choice of parameter αr_0 is taken as per the solid metal range. The critical properties of Cu, Na, and K are overestimated by our simulations and this indicates that the used parameters need to be refined to give a better agreement with experimental data. Scaling of the parameters to correctly predict the literature values, which are also observed to have a wide scatter, is reserved for further study.

Acknowledgments

References

[1] P.M. Morse, Phys. Rev. 34 (1929) 57–64.
[2] R.W. Keyes, J. Chem. Phys. 29 (1958) 523–530.
[3] R.C. Lincoln, K.M. Koliwad, P.B. Ghate, Phys. Rev. 157 (1967) 463–466.
[4] L.A. Girifalco, V.G. Weizer, Phys. Rev. 114 (1959) 687–690.
[5] A.R. Ruffa, Phys. Rev. B 24 (1981) 6915–6925.
[6] A.R. Ruffa, Phys. Rev. B 16 (1977) 2504–2514.
[7] H. Okumura, F. Yonezawa, J. Chem. Phys. 113 (2000) 9162–9168.
[8] R.A. Swalin, J. Phys. Chem. Solids 18 (1961) 290–296.
[9] F. Hensel, Phil. Trans. Roy. Soc. London A 356 (1998) 97–117.
[10] J.R. Errington, Phys. Rev. E 67 (2003), 012102/012101–012102/012104.
[11] B.A. Berg, T. Neuhaus, Phys. Rev. Lett. 61 (1992) 9–12.
[12] A.M. Ferrenberg, R.H. Swendsen, Phys. Rev. Lett. 61 (1988) 2635–2638.
[13] L.J. Van Poolen, C.D. Holcomb, V.G. Niesen, Fluid Phase Equilbr. 129 (1997) 105–111.
[14] H. Hess, Z. Metallkd. 89 (1998) 388–393.
[15] C.L. Yaws, Chemical Properties Handbook, McGraw-Hill, 1999.
[16] E.A. Avallone, T. Baumeister III, Marks' Standard Handbook for Mechanical Engineers, McGraw-Hill, 1996.
[17] G.R. Gathers, M. Ross, J. Non-Cryst. Solids 61–62 (1984) 59–64.
[18] P. Renaudin, C. Blancard, J. Clerouin, G. Faussurier, P. Noiret, V. Recoules, Phys. Rev. Lett. 91 (2003), 075002/075001–075002/075004.
[19] D. Bhatt, A.W. Jasper, N.E. Schultz, J.I. Siepmann, D.G. Truhlar, J. Am. Chem. Soc. 128 (2006) 4224–4225.
[20] A.V. Grosse, J. Inorg. Nuclear Chem. 24 (1962) 147–156.
[21] A.A. Likalter, Phys. Rev. B 53 (1996) 4386–4392.
[22] K. Boboridis, G. Pottlacher, H. Jager, Int. J. Thermophys. 20 (1999) 1289–1297.
[23] F. Hensel, J. Phys.: Condens. Matter 2 (1990) SA33–SA45.